Electronic Supplementary Information for

Competition between hydrogen bonds and van der Waals forces in intermolecular structure formation of protonated branched-chain alcohol clusters

Natsuko Sugawara,[1] Po-Jen Hsu,[2] Asuka Fujii,*[1] and Jer-Lai Kuo*[2]

[1]*Department of Chemistry, Graduate School of Science, Tohoku University, Sendai 980-8578, Japan*

[2]*Institute of Atomic and Molecular Sciences, Academia Sinica, Taipei 10617, Taiwan*

E-mail: asuka.fujii.c5@tohoku.ac.jp (A.F.), jlkuo@pub.iams.sinica.edu.tw (J.-L.K.).

Contents

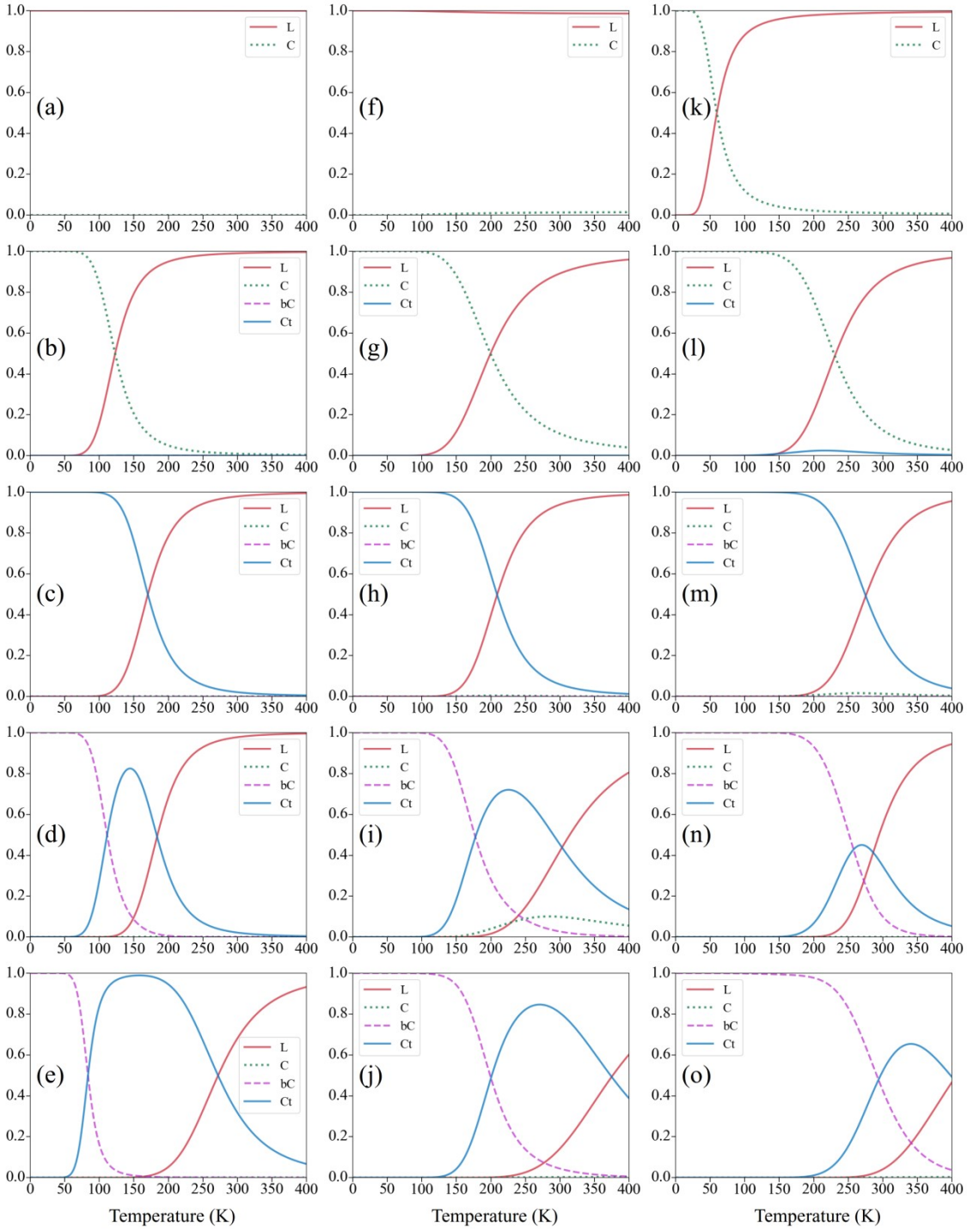

Fig. S1 Temperature-dependent relative population of $H^+(MeOH)_n$ (n = 4 (top) – 8 (bottom)). From the left to the right column, the levels of theory are B3LYP/6-31+G*, ωB97X-D/6-311+G(2d,p), and B3LYP/6-31+G*+D3.

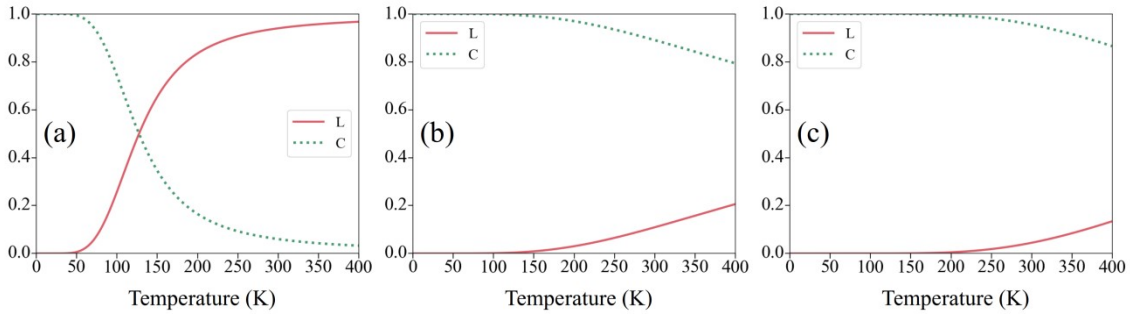

Fig. S2 Temperature-dependent relative population of $H^+(2\text{-PrOH})_4$. From the left to the right column, the levels of theory are B3LYP/6-31+G*, ωB97X-D/6-311+G(2d,p), and B3LYP/6-31+G*+D3.

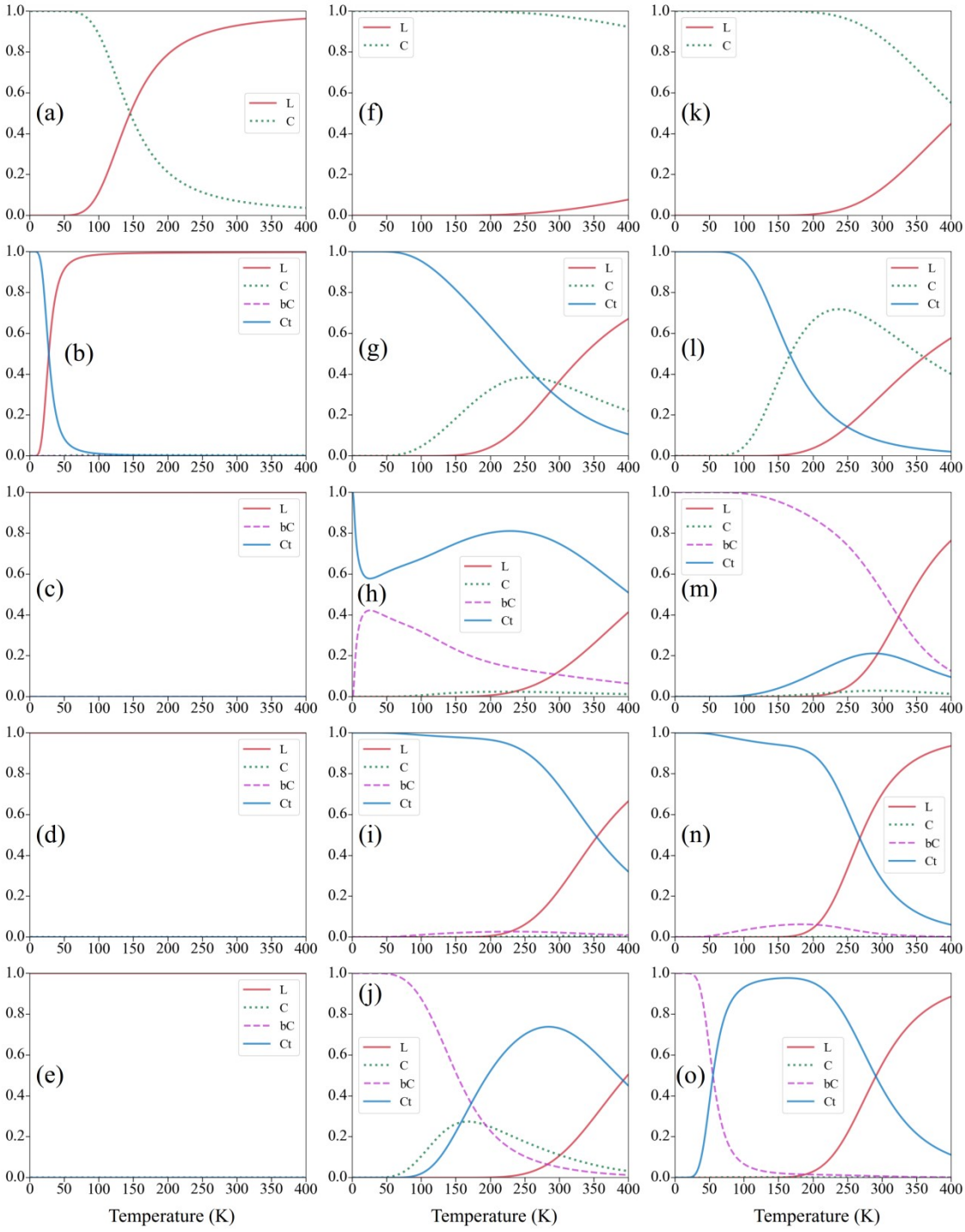

Fig. S3 Temperature-dependent relative population of $H^+(t\text{-BuOH})_n$ (n = 4 (top) – 8 (bottom)) From the left to the right column, the levels of theory are B3LYP/6-31+G*, ωB97X-D/6-311+G(2d,p), and B3LYP/6-31+G*+D3. In (c), (d), and (e), the relative population of the L structures are always 1 because they are much more stable than other structures.

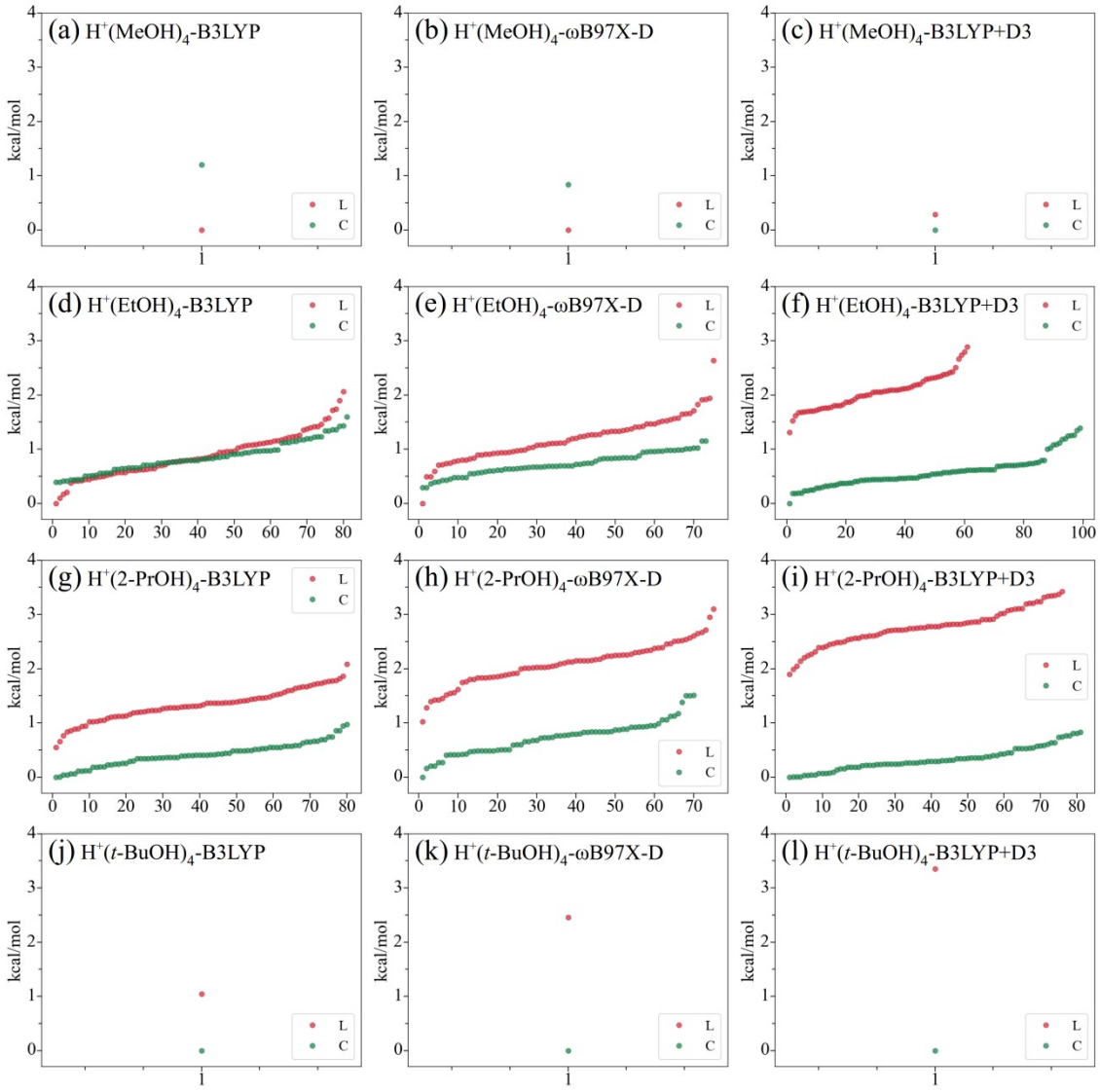

Fig. S4 The zero-point corrected relative energies of structurally distinct isomers of protonated alcohol tetramers. From top to bottom, $H^+(MeOH)_4$ (a-c), $H^+(EtOH)_4$ (d-f), $H^+(2\text{-}PrOH)_4$ (g-i), and $H^+(t\text{-}BuOH)_4$ (j-l). From the left to the right column, the levels of theory are B3LYP/6-31+G*, ωB97X-D/6-311+G(2d,p), and B3LYP/6-31+G*+D3. The abscissa is the numbering of the isomers. Two types of isomers are shown (**C** type = green and **L** type = red).

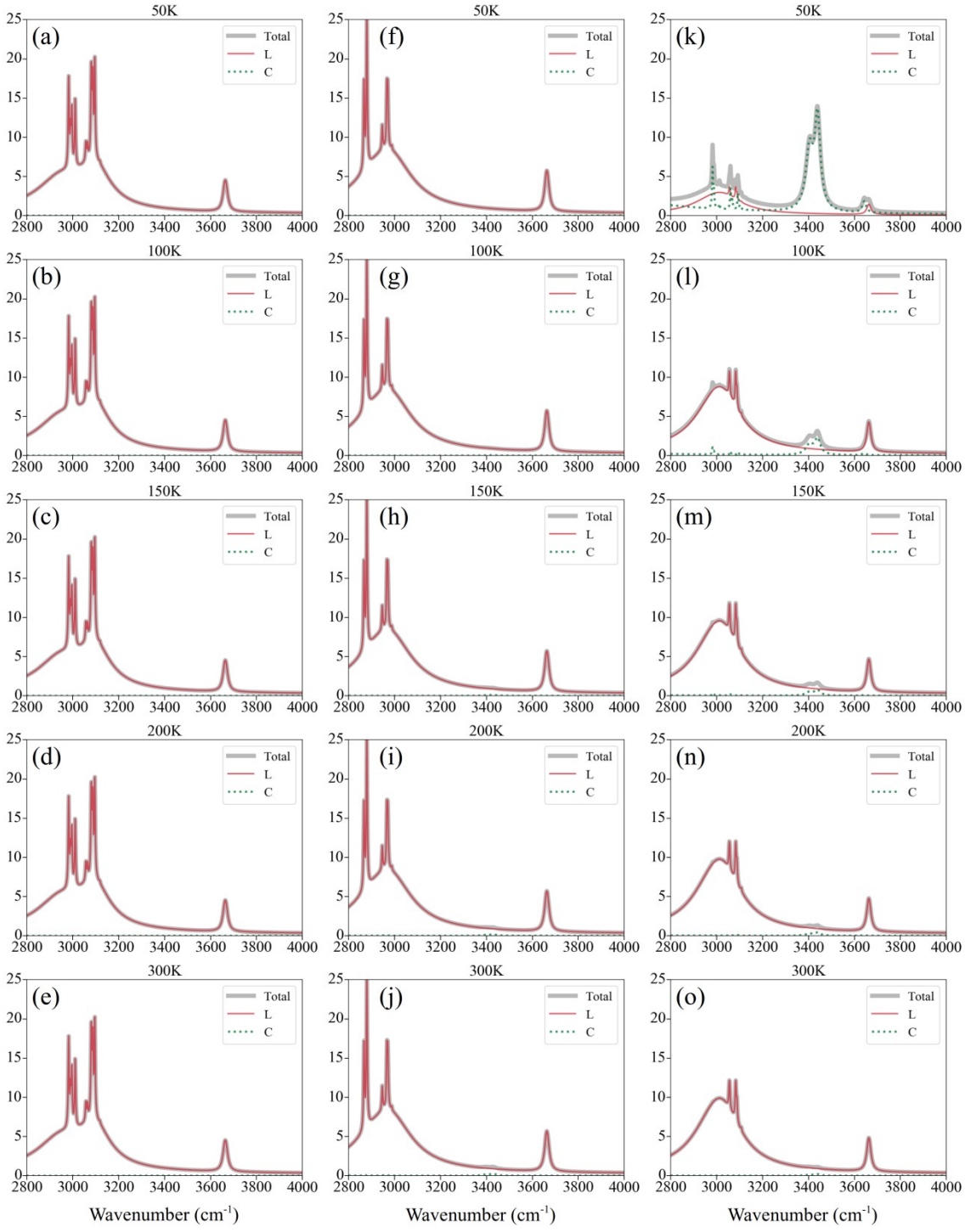

Fig. S5 Simulated IR spectra of $H^+(MeOH)_4$. From the left to the right column, the levels of theory are B3LYP/6-31+G*, ωB97X-D/6-311+G(2d,p), and B3LYP/6-31+G*+D3.

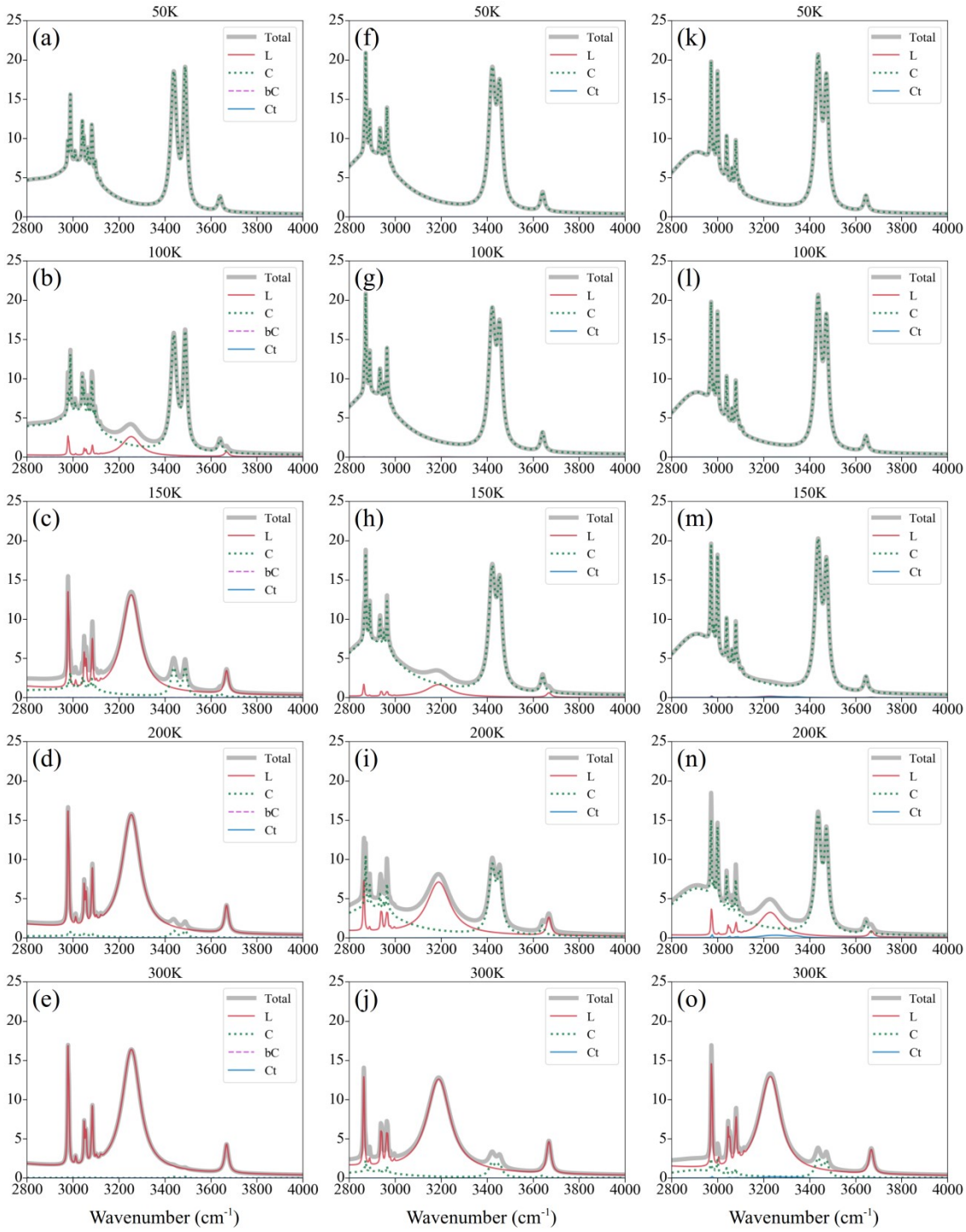

Fig. S6 Simulated IR spectra of $H^+(MeOH)_5$. From the left to the right column, the levels of theory are B3LYP/6-31+G*, ωB97X-D/6-311+G(2d,p), and B3LYP/6-31+G*+D3.

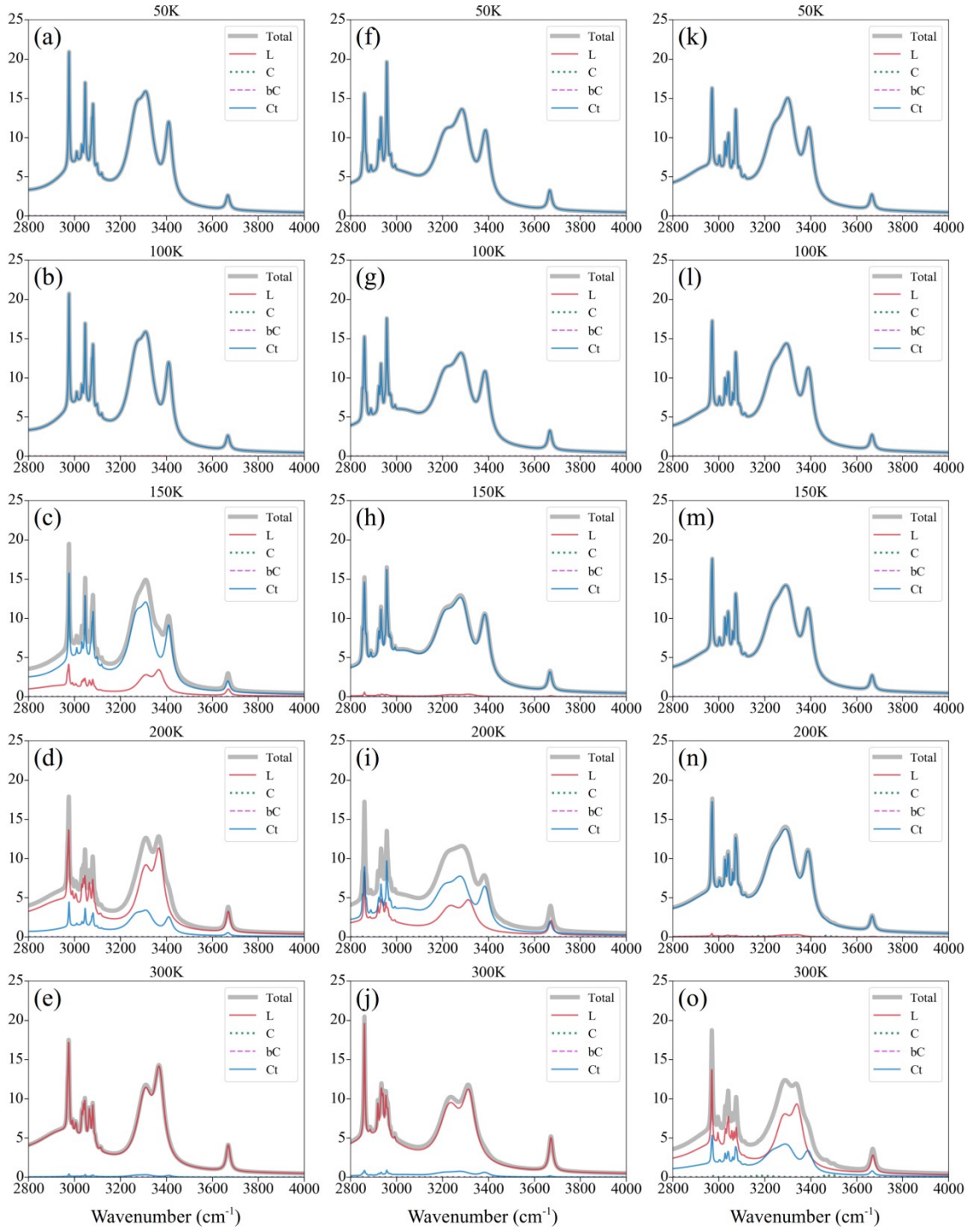

Fig. S7 Simulated IR spectra of $H^+(MeOH)_6$. From the left to the right column, the levels of theory are B3LYP/6-31+G*, ωB97X-D/6-311+G(2d,p), and B3LYP/6-31+G*+D3.

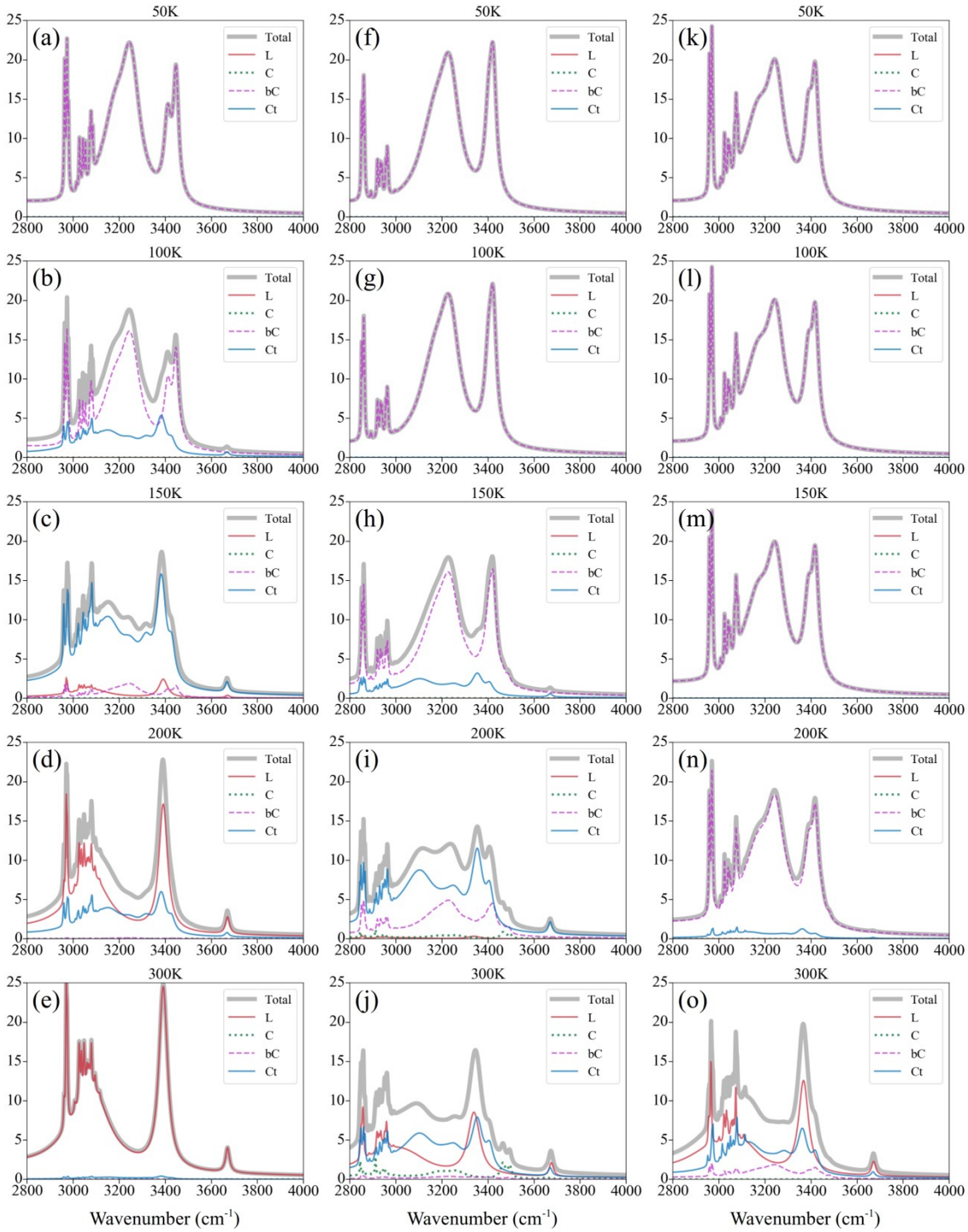

Fig. S8 Simulated IR spectra of $H^+(MeOH)_7$. From the left to the right column, the levels of theory are B3LYP/6-31+G*, ωB97X-D/6-311+G(2d,p), and B3LYP/6-31+G*+D3.

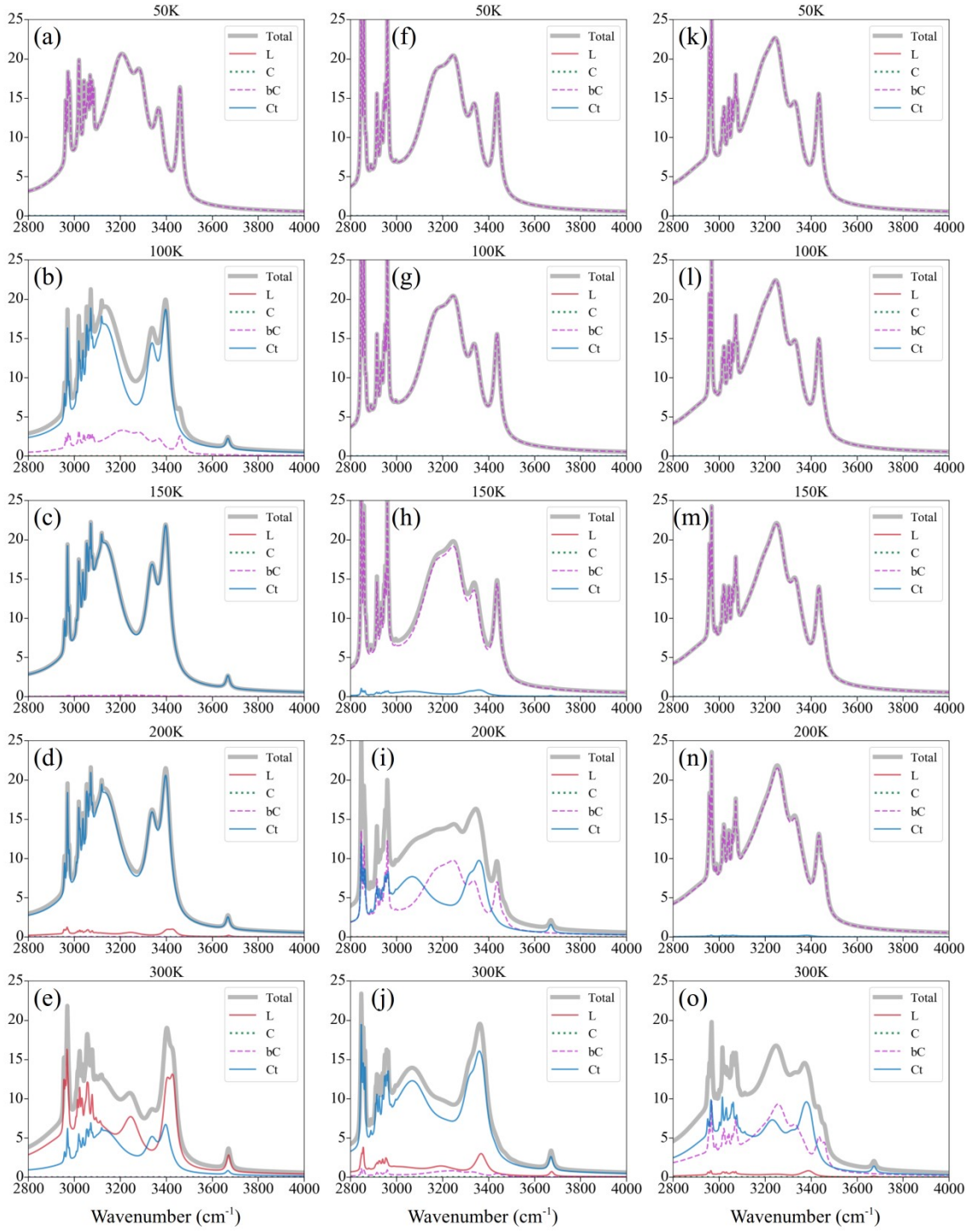

Fig. S9 Simulated IR spectra of $H^+(MeOH)_8$. From the left to the right column, the levels of theory are B3LYP/6-31+G*, ωB97X-D/6-311+G(2d,p), and B3LYP/6-31+G*+D3.

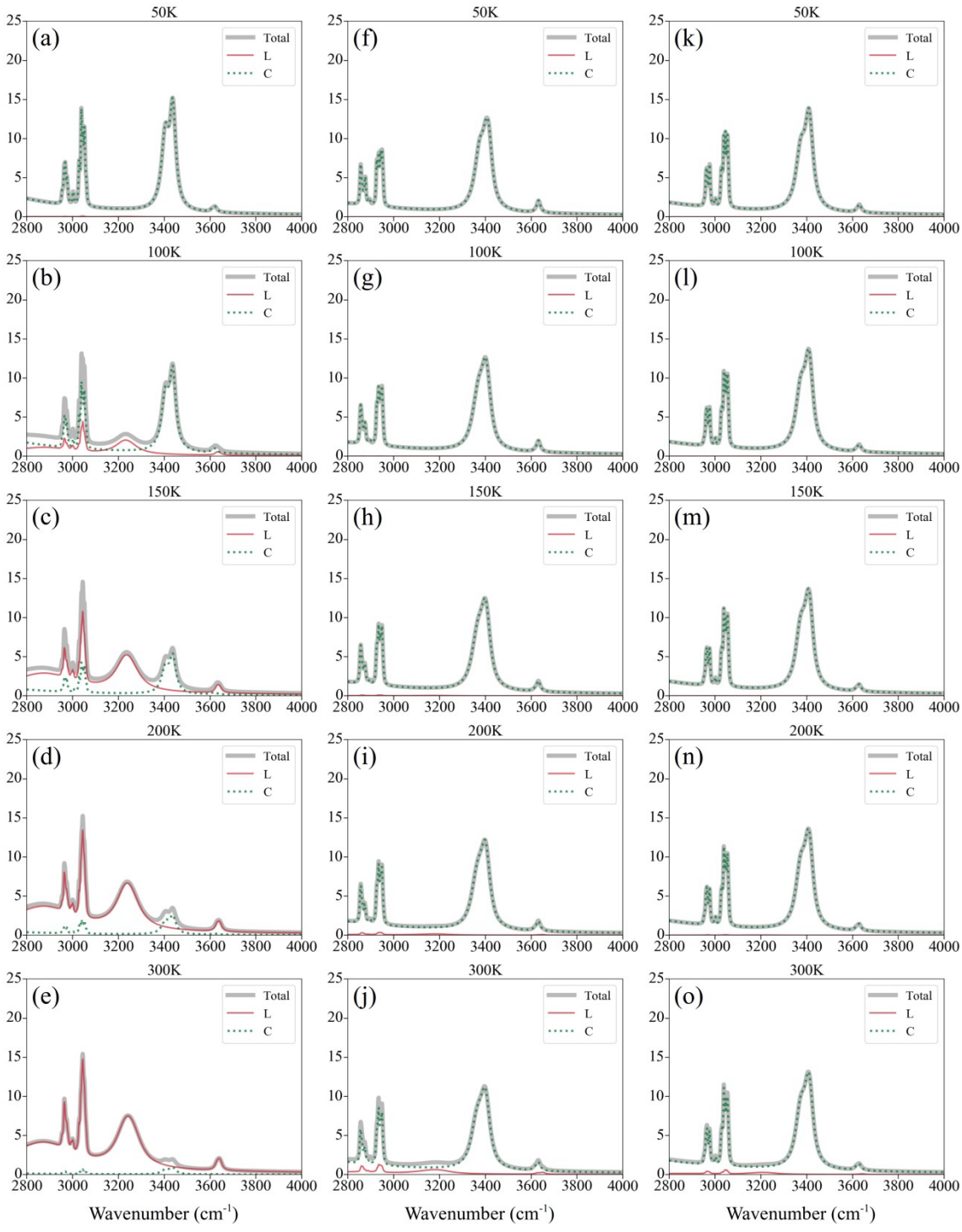

Fig. S10 Simulated IR spectra of $H^+(2\text{-PrOH})_4$. From the left to the right column, the levels of theory are B3LYP/6-31+G*, ωB97X-D/6-311+G(2d,p), and B3LYP/6-31+G*+D3.

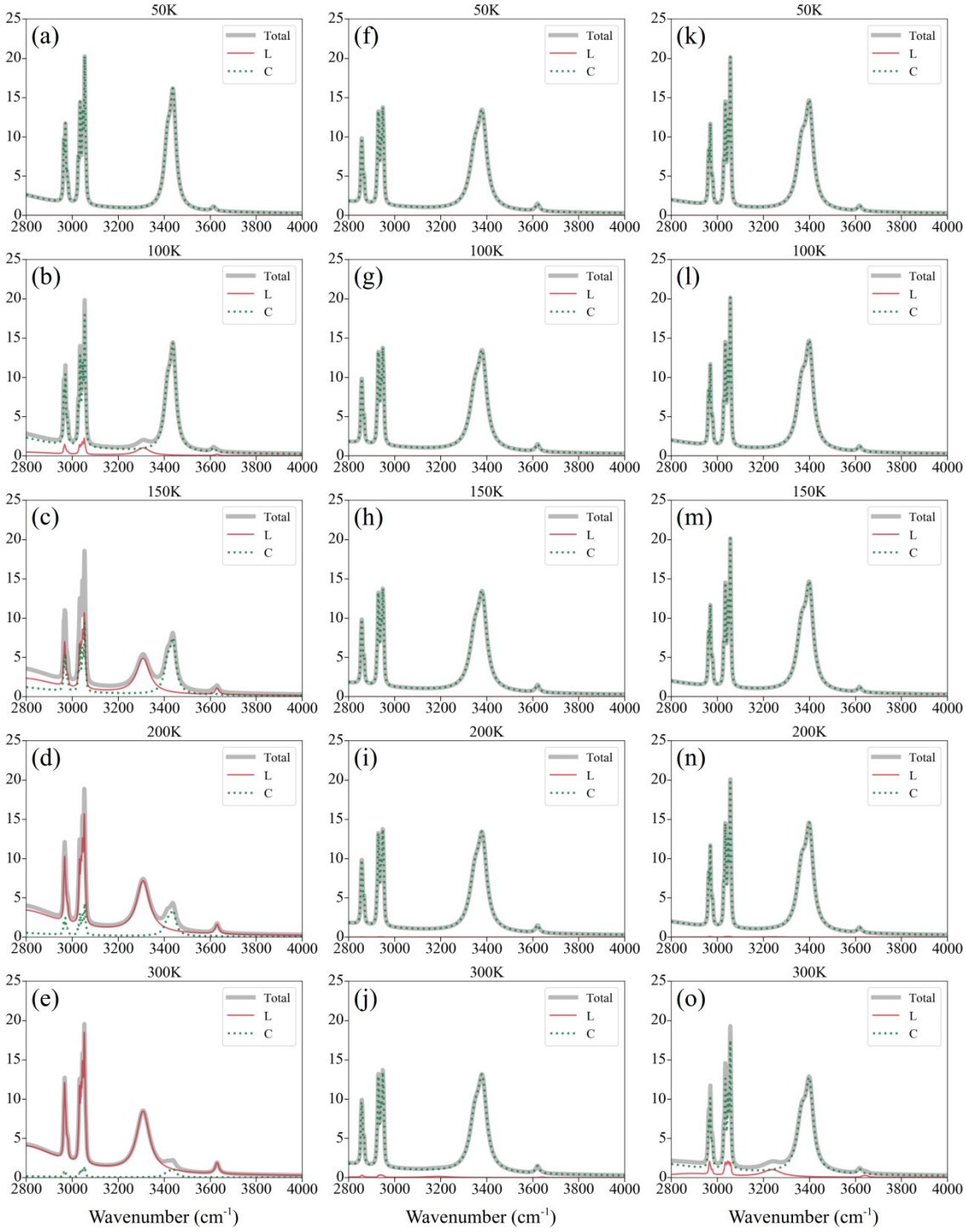

Fig. S11 Simulated IR spectra of H^+(*t*-BuOH)$_4$. From the left to the right column, the levels of theory are B3LYP/6-31+G*, ωB97X-D/6-311+G(2d,p), and B3LYP/6-31+G*+D3.

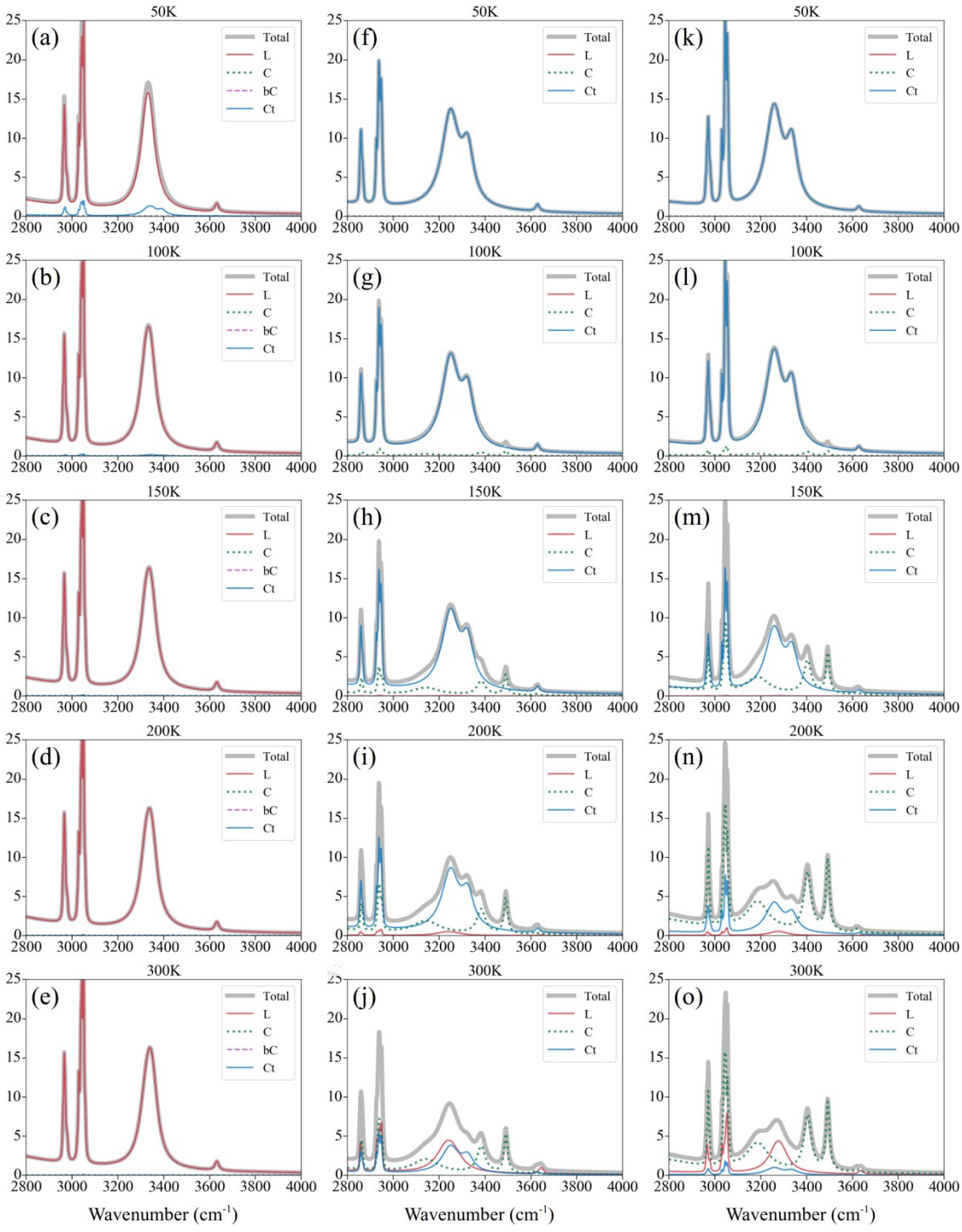

Fig. S12 Simulated IR spectra of $H^+(t\text{-BuOH})_5$. From the left to the right column, the levels of theory are B3LYP/6-31+G*, ωB97X-D/6-311+G(2d,p), and B3LYP/6-31+G*+D3.

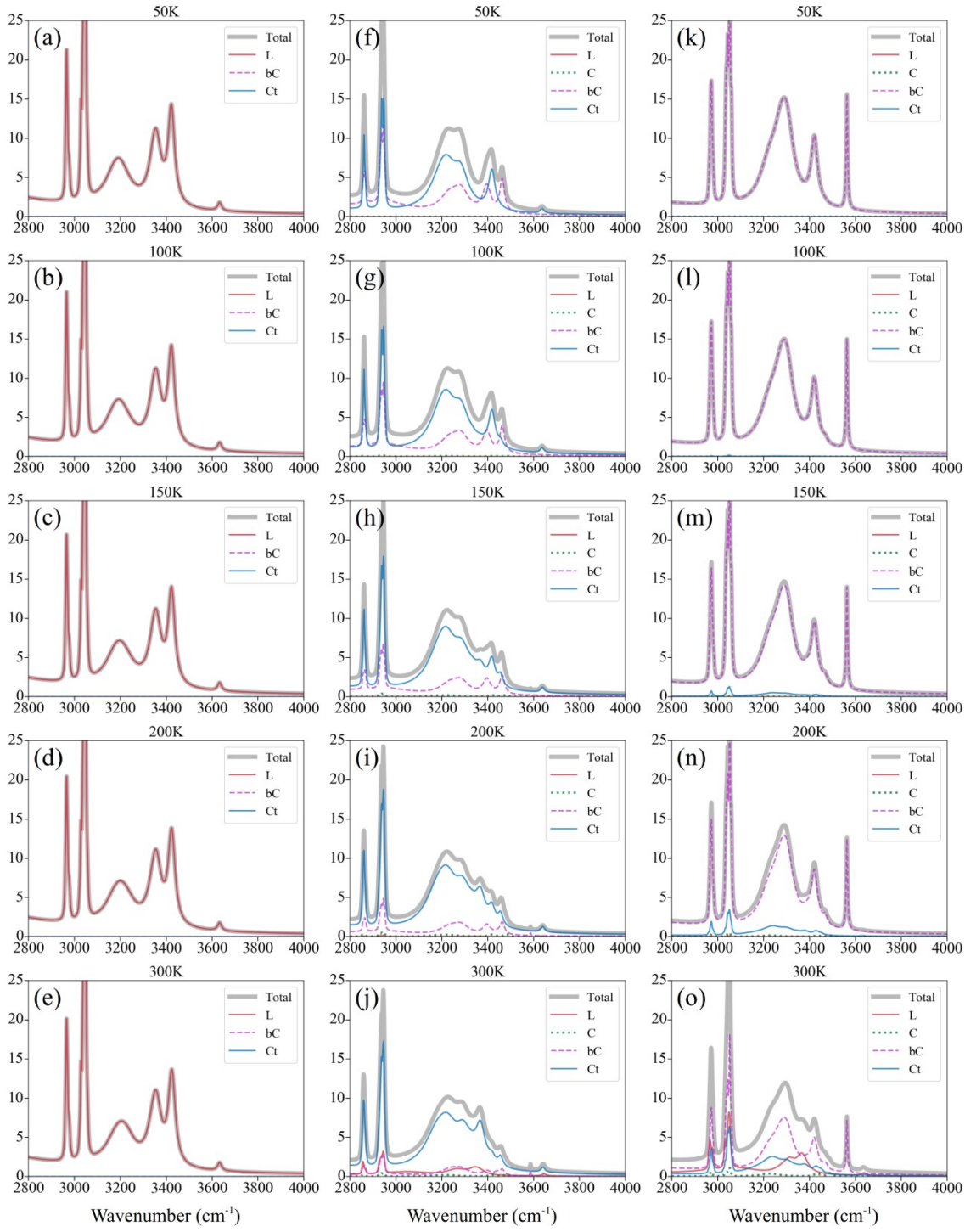

Fig. S13 Simulated IR spectra of $H^+(t\text{-BuOH})_6$. From the left to the right column, the levels of theory are B3LYP/6-31+G*, ωB97X-D/6-311+G(2d,p), and B3LYP/6-31+G*+D3.

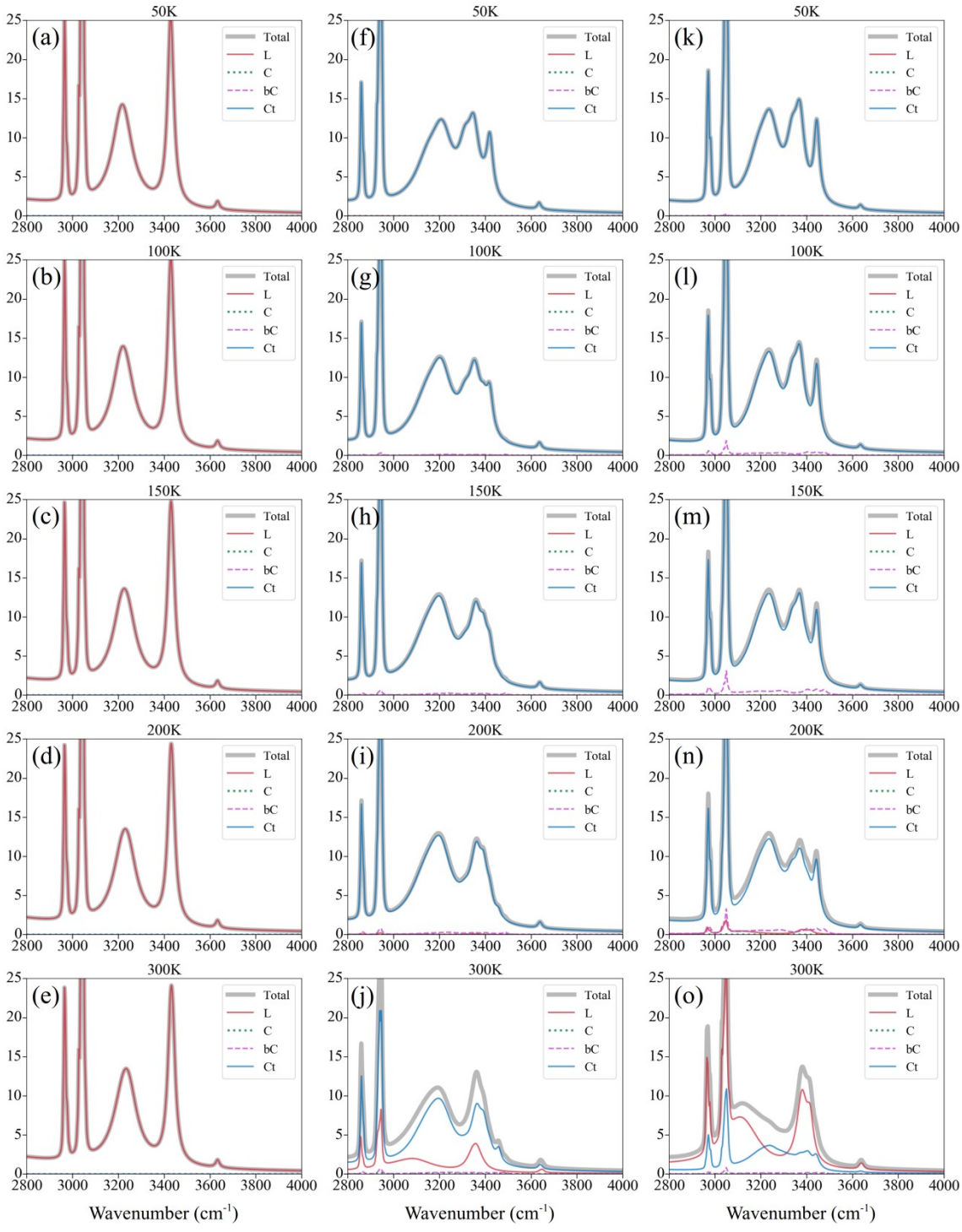

Fig. S14 Simulated IR spectra of $H^+(t\text{-BuOH})_7$. From the left to the right column, the levels of theory are B3LYP/6-31+G*, ωB97X-D/6-311+G(2d,p), and B3LYP/6-31+G*+D3.

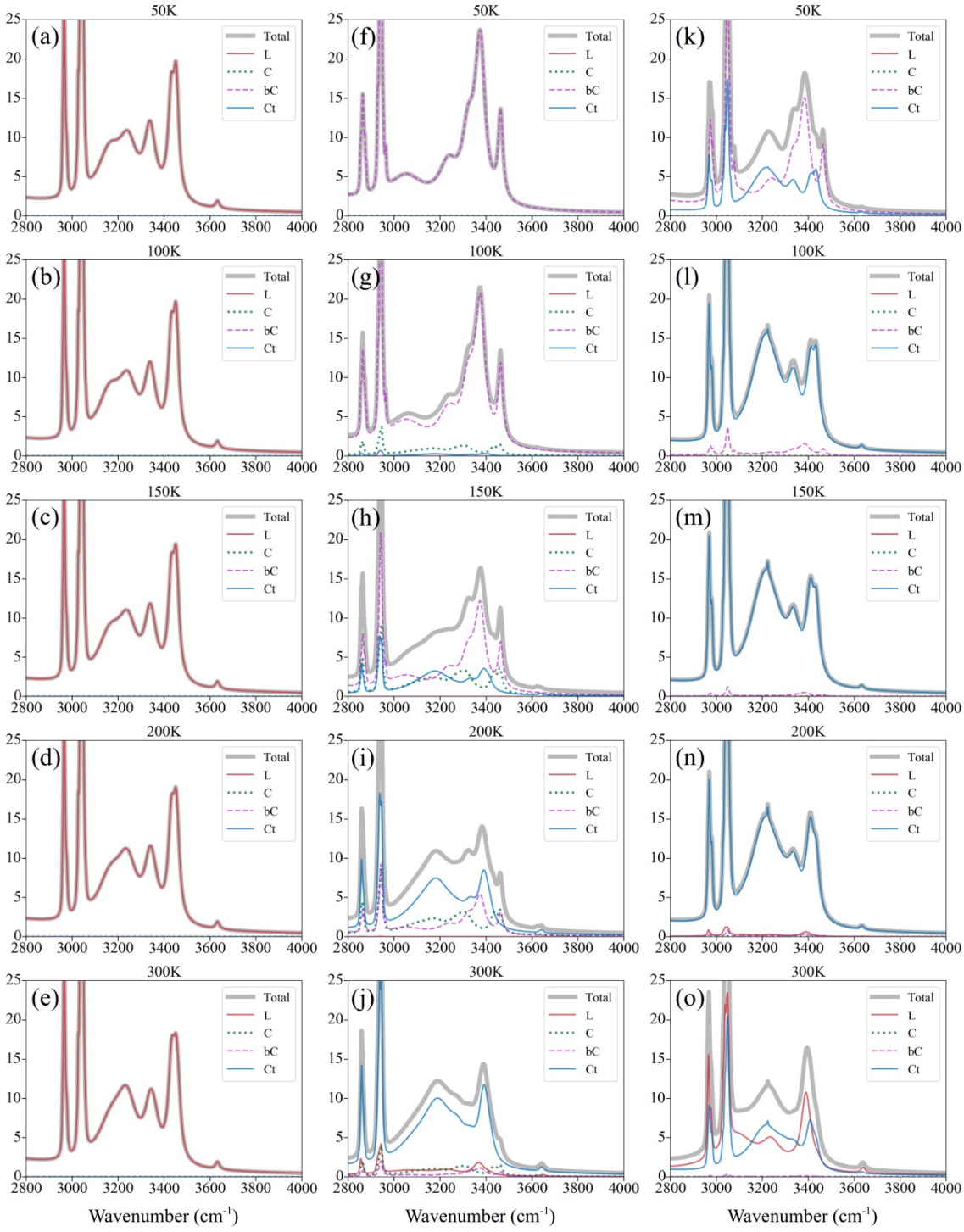

Fig. S15 Simulated IR spectra of $H^+(t\text{-BuOH})_8$. From the left to the right column, the levels of theory are B3LYP/6-31+G*, ωB97X-D/6-311+G(2d,p), and B3LYP/6-31+G*+D3.

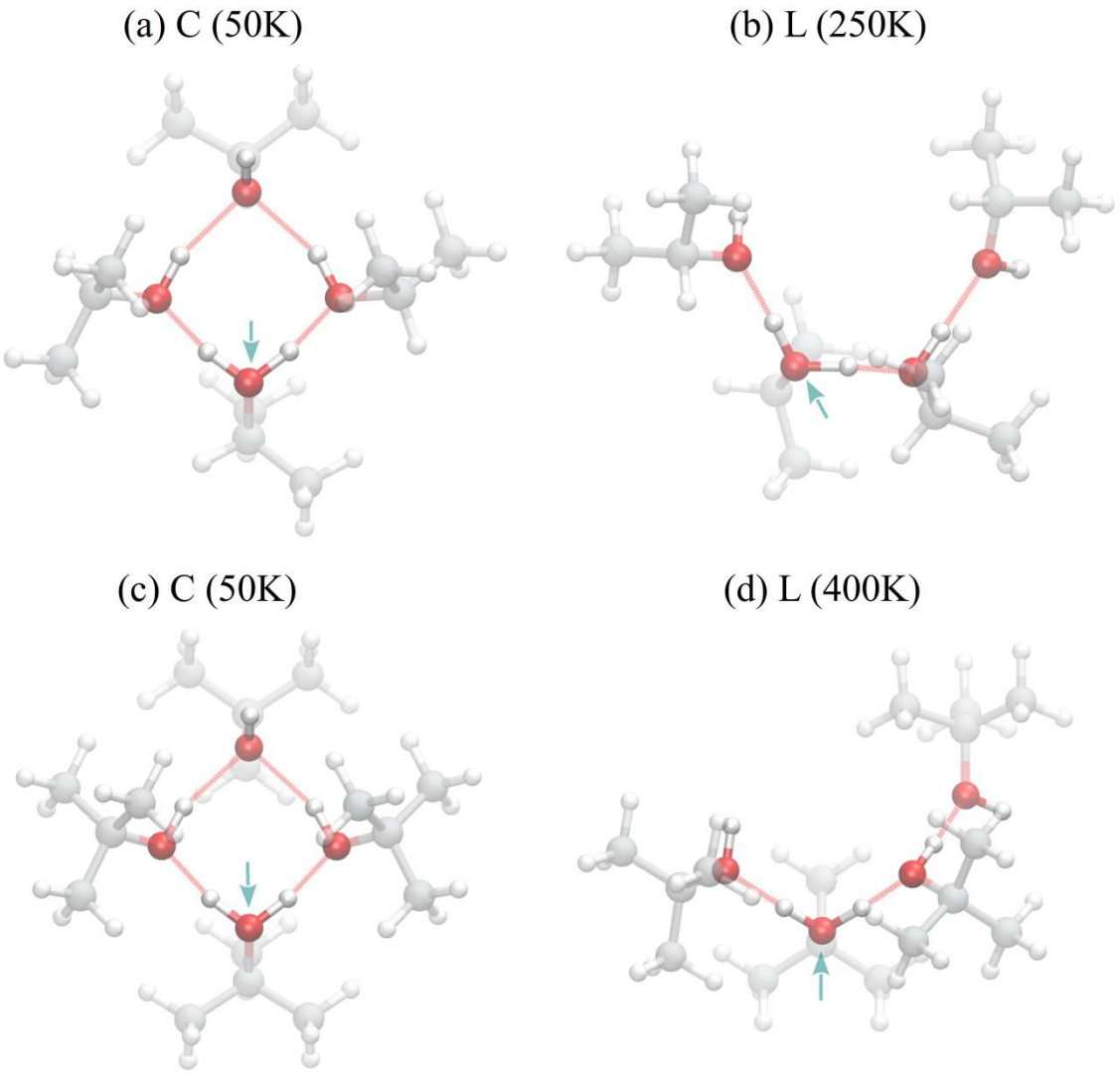

Fig. S16 The minimum free energy isomer structures of $H^+(2\text{-PrOH})_4$-B3LYP (a and b) and $H^+(t\text{-BuOH})_4$-B3LYP (c and d). The former is represented by (a) **C** structure at 50K and (b) **L** structure at 250K. The latter is represented by (c) **C** structure at 50K and (b) **L** structure at 400K. The corresponding zero-point corrected relative energies are (a) 0.064, (b) 0.656, (c) 0 and (d) 1.045 kcal/mol.

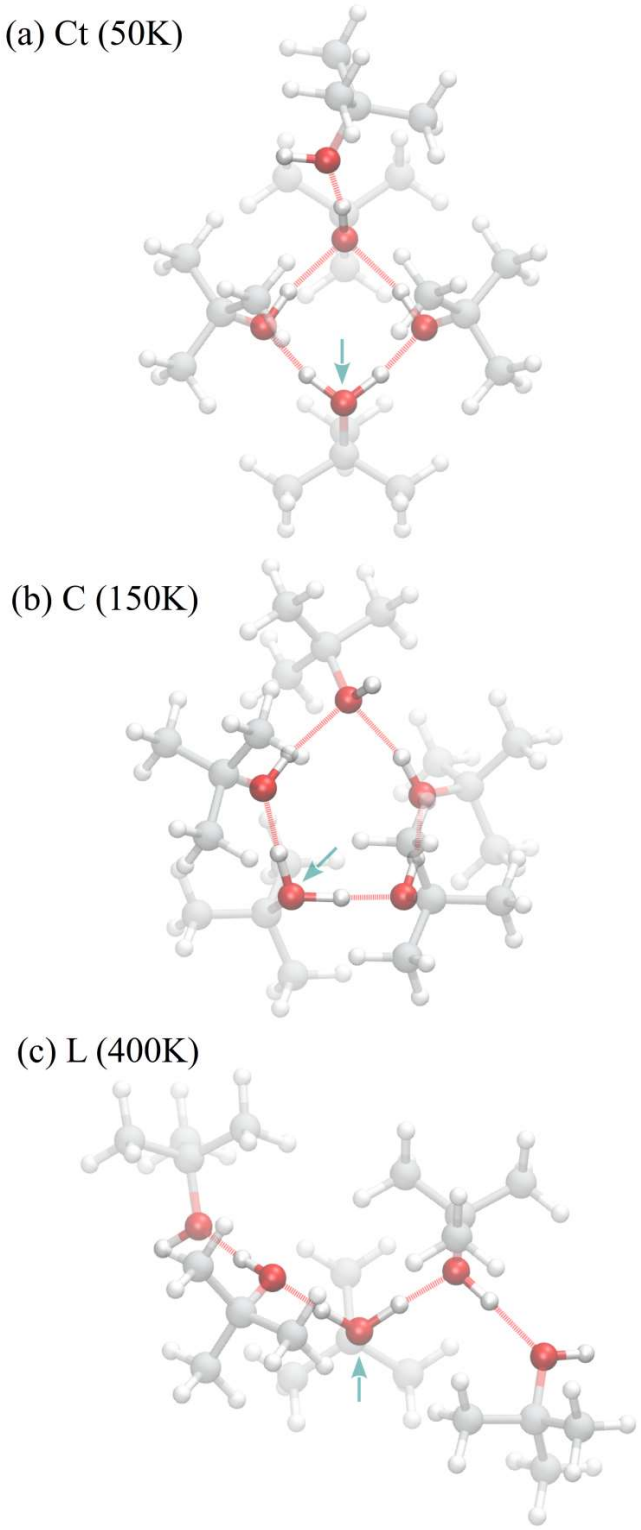

Fig. S17 The minimum free energy structures of H^+(*t*-BuOH)$_5$-B3LYP+D3. From (a) to (c) are **Ct** structure at 50K, **C** structure at 150K, and **L** structure at 400K. The corresponding zero-point corrected energies are (a) 0, (b) 1.211, and (c) 3.423 kcal/mol.

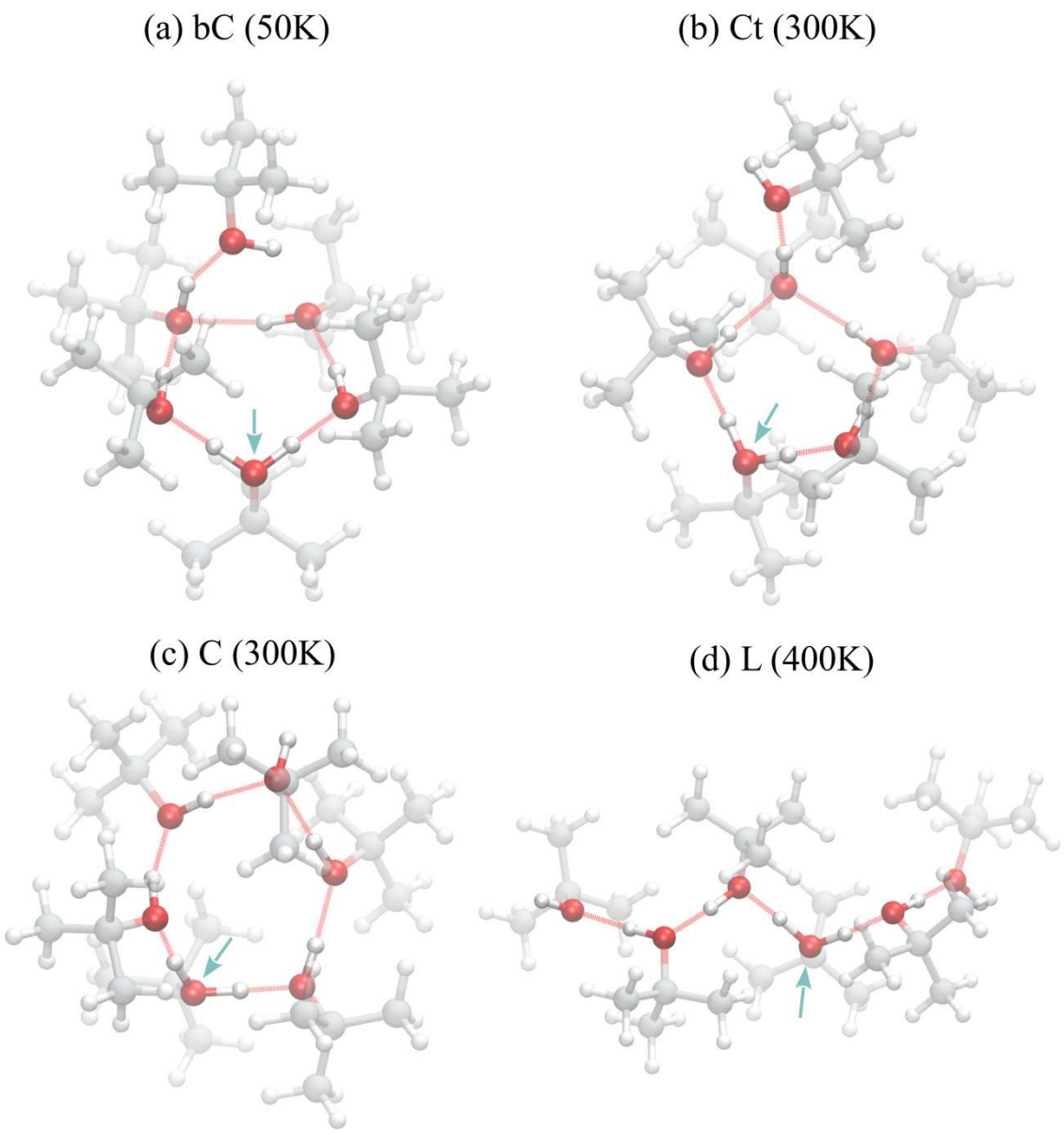

Fig. S18 The minimum free energy structures of H^+(*t*-BuOH)$_6$-B3LYP+D3. From (a) to (d) are **bC** structure at 50K, **Ct** and **C** structures at 300K, and **L** structure at 400K. The corresponding zero-point corrected energies are (a) 0, (b) 1.086, (c) 1.588, and (d) 4.923 kcal/mol.

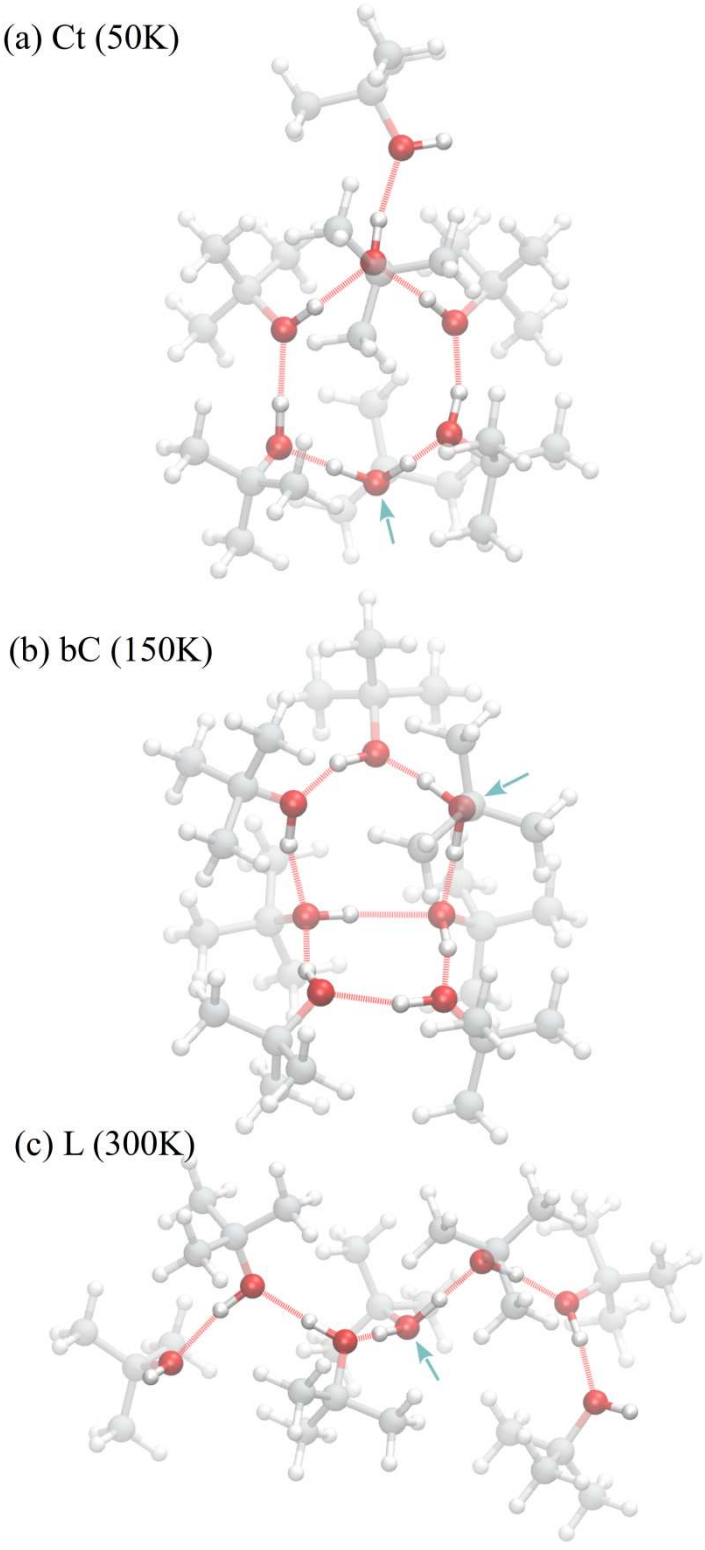

Fig. S19 The minimum free energy structures of $H^+(t\text{-BuOH})_7$-B3LYP+D3. From (a) to (c) are **Ct** structure at 50K, **bC** structure at 150K, and **L** structure at 300K. The corresponding zero-point corrected energies are (a) 0, (b) 0.462, and (c) 4.268 kcal/mol.

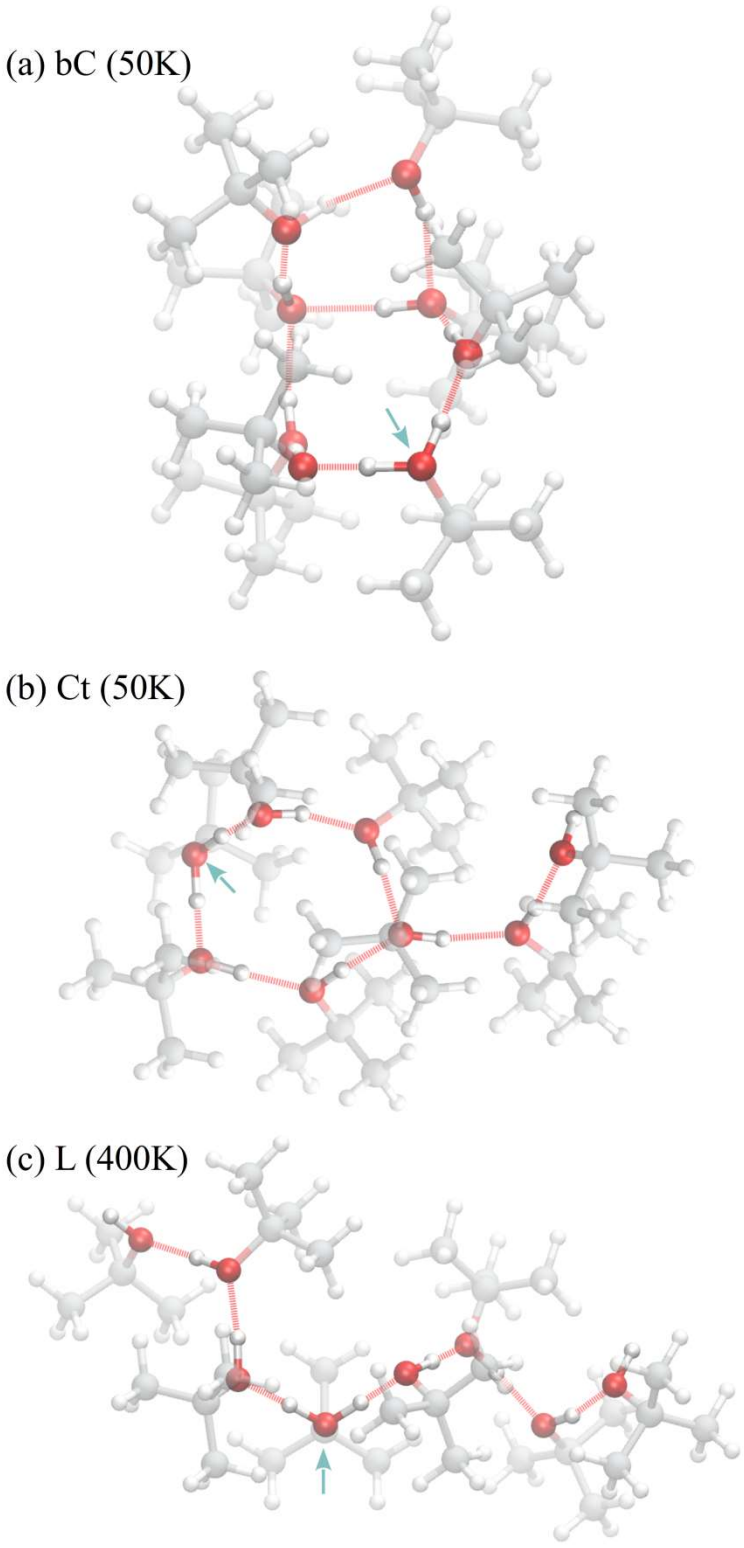

Fig. S20 The minimum free energy structures of $H^+(t\text{-BuOH})_8$-B3LYP+D3. From (a) to (c) are **bC** and **Ct** structures at 50K and **L** structure at 400K. The corresponding zero-point corrected energies are (a) 0, (b) 0.31, and (c) 4.172 kcal/mol.